Available online at www.sciencedirect.com

ScienceDirect

Physics Procedia 5 (2010) 137–146

Physics Procedia

www.elsevier.com/locate/procedia

LANE 2010

Experimental and Numerical Optimization of Beam Shapes for Short-Pulse Ultraviolet Laser Cutting Processing

Anatoly Sotnikov[a,b]*, Harald Laux[a], Bernd Stritzker[b]

[a]*OSRAM Opto Semiconductors GmbH, Leibnizstrasse 4, 93055 Regensburg, Germany*
[b]*University of Augsburg, Institute of Physics, Universitaetsstrasse 1, 86159 Augsburg, Germany*

Abstract

In this work the effect of elliptical beam shapes on cutting performance of silicon is studied experimentally using a Diode Pumped Solid State Q-switched UV laser operating at the wavelength of 355 nm. Elliptical beams are investigated by varying scanning speed, repetition rate and average output power. It is shown that a short elliptical beam with 6 x 230 µm dimension forms a deeper groove at higher cutting speed and lower average output power compared to a longer elliptical beam. A numerical model of the laser cutting process is also described. Some validation results for single and multi-pulse cutting are shown.

Keywords: process optimization; laser-based cutting of silicon; laser cutting simulation

1. Introduction

One of the main advantages in laser cutting is its low heat-affected zone (HAZ) region and low groove width which leads to low or no thermal distortion. To optimize laser cutting processes it is necessary to have thorough knowledge of the HAZ, groove width and the material thickness that can be cut.

Considerable research has been carried out and many experimental results and some numerical models of laser cutting processes are found in the literature. Karnakis et al. [1] presented experimental results of micro-machining of polymers and silicon nitride using reshaped pulsed Gaussian laser beam. A review of an IR pulsed laser cutting simulation was presented by Fell et al. [2]. Zhang and Faghri [3] developed a theoretical model to predict the cavity formation for UV laser micro-machining with nanosecond pulse duration. Sundar [4] proposed the first CFD (Computational Fluid Dynamics) based model for CW laser cutting with phase changes during cutting process.

In this work the effect of beam shape variation at various process parameters is studied experimentally using a

* Corresponding author.
E-mail address: anatoly.sotnikov@osram-os.com

1875-3892 © 2010 Published by Elsevier B.V. Open access under CC BY-NC-ND license.
doi:10.1016/j.phpro.2010.08.130

pulsed UV laser. It was found that at low repetition rate of 10 kHz the effect of beam shape variation toward shorter beams has almost no positive effect on cutting performance. On the contrary, the groove is getting wider and its depth shallower. But at higher repetition rates of 20 – 25 kHz, a deeper cut is achieved with higher cutting speed and lower output power.

A numerical model for single and multi-pulse cutting is also presented. The model is developed within the commercial CFD code Fluent. It is capable of simulating the formation of a cutting groove under the irradiation of a pulsed laser beam with various beam shape profiles and laser parameters. Some validation results are shown.

2. Experimental Set-up and Beam Profile Analysis

A high-power Nd:YAG Q-switched diode-pumped laser with its fundamental frequency tripled ($\lambda = 355$ nm) was used as the UV energy source for the experiments. The laser is operated at repetition rates ranging from 10 to 25 kHz. The pulse duration of the output beam is 35 to 61 ns depending on the repetition rate. The maximum output power used in this study is 8 W. The output beam profile has elliptical shape. The beam shape is varied by changing the distance between two cylindrical lenses. Two beam shapes with 6 x 230 µm and 6 x 460 µm are used. The laser micro-machining system includes the UV laser source, beam expander, unit for beam length adjustment, optical focusing system and a beam profiler (Fig. 1).

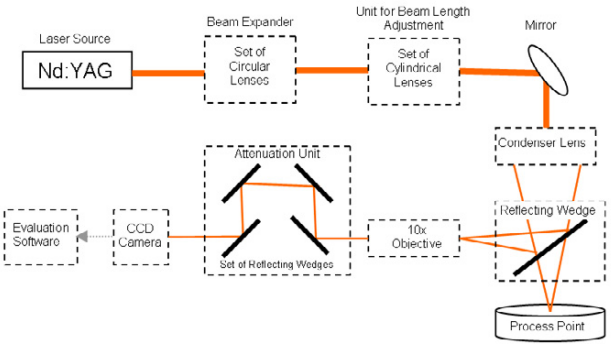

Fig. 1. Experimental set-up of laser system and beam profiler

Knowledge of the beam shape profile at process point is required for laser intensity and overlapping degree calculation. Because the laser beam at process point has high intensity, it is necessary to attenuate the laser beam before measuring it with an electronic instrument. The attenuation method is based on the principle that part of the light is reflected on optical surfaces. For the given set-up a total attenuation factor of $5 \cdot 10^7$ is used.

The focused laser beam spot at process point is smaller than 10 µm in width. Since camera pixels, at the smallest, are approximately 6 - 7 µm, the camera alone can not be used effectively for measuring the focused spots and a 10x objective lens is placed in front of the attenuation unit and CCD sensor for magnification of the beam spot.

From the beam profile analysis the width and the length of elliptical beams are taken. The cutting quality and groove geometry were examined using an optical microscope and a Scanning Electron Microscope.

3. Theoretical Background

3.1 Beam divergence consideration

When a Gaussian beam is focused with a lens, the size of the beam becomes minimal at the focal plane of the lens. This minimum size is referred to as the beam waist. Because of diffraction, the focused laser beam spreads and does not remain focused as it propagates away from the beam waist in free space. The radius of a Gaussian laser beam, $w(z)$ at a distance z from the axial location of the beam waist measured along the beam axis, is given by [5]:

$$w^2(z) = w_0^2\left[1+\left(\frac{\lambda z}{\pi w_0^2}\right)^2\right] \quad (1)$$

where λ is the wavelength of the laser and w_0 is the radius of the beam waist.

For the given laser system with an elliptical beam with Gaussian distribution along major and minor axes, the effect of laser beam propagation (divergence) along the short and long axes was calculated (Eq. 1) and was measured with the beam profiler.

The calculated and measured beam widths are in good agreement (Fig 2a). Moreover, due to the fact that the beam waist for long axis lies at -6000µm defocus, the beam length does not change drastically within the range of -150 to +150 µm focal plane position (Fig. 2b).

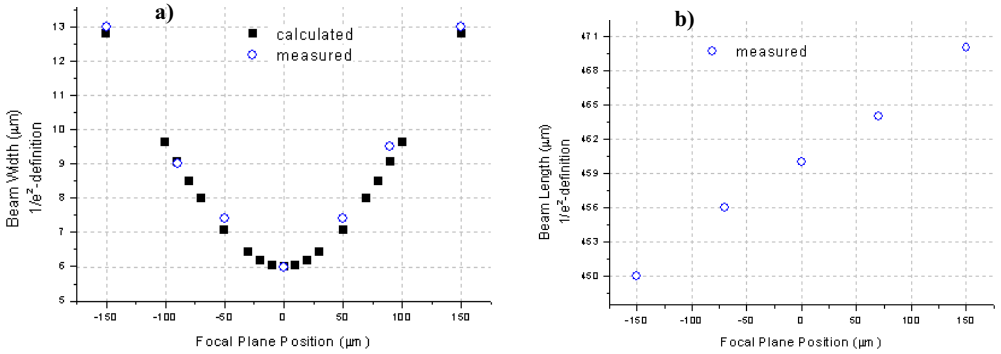

Fig. 2. Divergence of beam width (a) and beam length (b) along focal plane position

The results show that for final depths below 20 µm the divergence effect on width and length can be neglected.

3.2 Laser intensity distribution

The intensity distribution of the moving laser beam obeys the Gaussian distribution laws and thus is considered as spatially Gaussian [6]:

$$I(x,y,z,V) = (1-R)\frac{2P_0}{\pi x_z(z) y_z(z)} \cdot \exp\left[-2\left(\frac{x}{x_z(z)}\right)^2\right] \cdot \exp\left[-2\left(\frac{y+d(V)}{y_z(z)}\right)^2\right] \quad (2)$$

where R is the reflectivity of silicon [7], P_0 is the peak power, x_z and y_z are the waist radii of the beam along major and minor axes at distance z from the top surface, respectively, while x and y are the distances from the center and d is the spatial distance between pulses (Eq. 10). The waist radii, x_z and y_z at distance z from the top surface are given by Eq. 1 such that Eq. 2 includes the effect of the beam divergence distribution.

4. Numerical model

During cutting with a pulsed laser, the target material is first heated from ambient to melting temperature and then evaporated by additional heating when its temperature reaches the vaporization point. Moreover, in-between two consecutive pulses (pulse-off time) the material cools down over a period much longer (factor of 10^3) compared

to the pulse duration. Here, a numerical model for this process is presented. The model is developed within the commercial CFD software Fluent using its solidification capacity [8].

The main model assumptions are: *(i)* the surface heat flux due to the laser irradiation is known (Eq. 2); *(ii)* plasma in the gas phase does not form; *(iii)* the laser energy that is not reflected at the material surface is completely absorbed at the surface; *(iv)* the cutting process is modelled as a sublimation process (melt pool is negligible in extend); *(v)* convection in the gas phase is approximated by a high effective conductivity.

The primary model variables are the total enthalpy, H, the temperature, T, and the so-called liquid fraction, β, which is defined as the local fraction of liquid (here gas), while 1- β is the local solid fraction. The solid interface is defined as the contour at which β equals 0.5.

The equation for the total enthalpy is:

$$\frac{dH}{dt} = \nabla k \nabla T \tag{3}$$

where k is the thermal conductivity, and where the total enthalpy is defined as:

$$H = h_0 + \int_{T_0}^{T} C_p dT + \beta \Delta L \tag{4}$$

Here, ΔL is the latent heat of sublimation, Cp is the heat capacity of the material and index 0 denotes reference properties. The relationship between liquid fraction and temperature is given by:

$$\beta = \begin{cases} 0 & T < T_S \\ \dfrac{T - T_S}{T_L - T_S} & T_S < T < T_L \\ 1 & T > T_L \end{cases} \tag{5}$$

where T_S and T_L are solidus and liquidus temperatures, respectively.

To obtain solutions for the equation system, boundary conditions have to be given at the three surface types of the model: wall, irradiated surface and symmetry plane (Fig. 3). Here, zero flux and constant temperature conditions are used:

$$\left.\frac{\partial T}{\partial n}\right|_{sym} = 0, \quad T\big|_{wall} = T_\infty \tag{6}$$

at symmetry plane and walls, respectively, where n is the surface normal and T_∞ is the ambient temperature. At the irradiated surface the surface heat flux is specified:

$$q_{surf} = \left\{ \begin{array}{ll} I(x,y,z,V) - h\left(T_{surf} - T_\infty\right) - \varepsilon\sigma\left(T^4{}_{surf} - T^4{}_\infty\right) & pulse-on\ time \\ -h\left(T_{surf} - T_\infty\right) - \varepsilon\sigma\left(T^4{}_{surf} - T^4{}_\infty\right) & pulse-off\ time \end{array} \right\} = -k\left.\frac{\partial T}{\partial n}\right|_{surface} \tag{7}$$

where h is an external heat transfer coefficient, ε is the emissivity and σ is the Stefan-Boltzmann constant The laser-induced surface heat flux *I(x,y,z,V)* is given by Eq. (2). For the present laser settings convective and radiation cooling are small compared to laser intensity (*I)* during the pulse-on time and therefore neglected in the following (last two terms in Eq. (7) for pulse-on time).

A simulation is initialized with ambient temperature in the entire wok piece.
Simulation of the pulse-off time has confirmed that the work piece temperature cools down to ambient temperature, thus the term cooling period.

Now, the algorithm that has been used to simulate single- and multi-pulse regimes is described. In general the mesh is not deformed during a pulse. Thus, a region develops on the mesh which is filled with gas. For single-pulse cutting the simulation is stopped after the first pulse and the groove shape is given by the contour of $\beta = 0.5$. For multi-pulse cutting the region filled with gas ($\beta > 0.5$) is cut away after each pulse and a new mesh is generated on the new geometry. Then the temperature is initialized and the new irradiated surface boundary condition is imposed (Eq. (2) and Eq. (10) – including effect of work piece movement). Then the next pulse is simulated. Again, the region filled with gas is cut away and the procedure is repeated until the final depth is reached. Final and intermediate groove shapes are given by the contour of $\beta = 0.5$.

Materials properties are given in Table 1. Even if a pure material is cut a small solidification interval is introduced, bounded by solidus and liquidus temperature and centred on the sublimation temperature (Table 1). Materials properties vary linearly over this interval from solid to gas phase properties. Note that the predicted cutting depth has proved to be independent of the gas phase conductivity (dependent only on the laser intensity and work piece speed). However, the temperature distribution in the gas is affected by the conductivity. Its value was set to an artificially high value to accommodate convective and radiation effects in the groove below the irradiated surface, and to bring down the gas phase temperature to a realistic level.

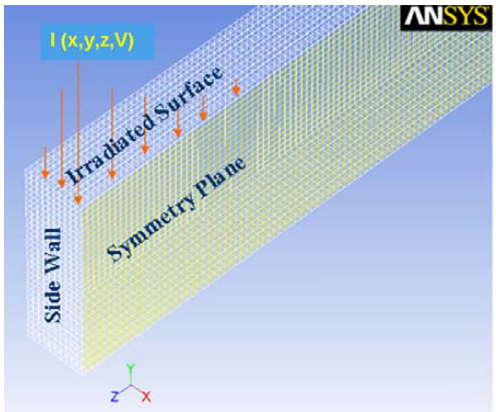

Fig. 3. Boundaries and mesh used for the simulations (CFD modelling)

Table 1. Constant materials properties and model parameters

T_S, K	T_L, K	T_{sub}, K	k_{gas}, J/kg-K	k_{solid}, J/kg-K	C_{Pgas}, W/m-K	C_{Psolid}, W/m-K
2626	2631	2628,5	300[1]	148	1000	714

[1]Artificially high to accommodate convection and radiation effects in the groove.

5. Results

5.1 Single-pulse regime

Single pulses were performed experimentally to study the dependency between laser output power and groove shape. All single pulse shots were made at 35 ns pulse width. The only parameter that was changed is the average output power. Measured and simulated groove shapes for various output powers are presented in Figs. 4 and 5.

The experimentally measured groove depths are 2.2, 3.5 and 4.6 µm at 2, 5 and 8 W output power, respectively, and the groove widths are 7, 9 and 11 µm at 2 W, 5 W and 8 W output power, respectively (Fig. 4a-f). The simulated groove length at 5 W is equal to 425 µm compared to 435 µm measured (Fig. 4g, h).

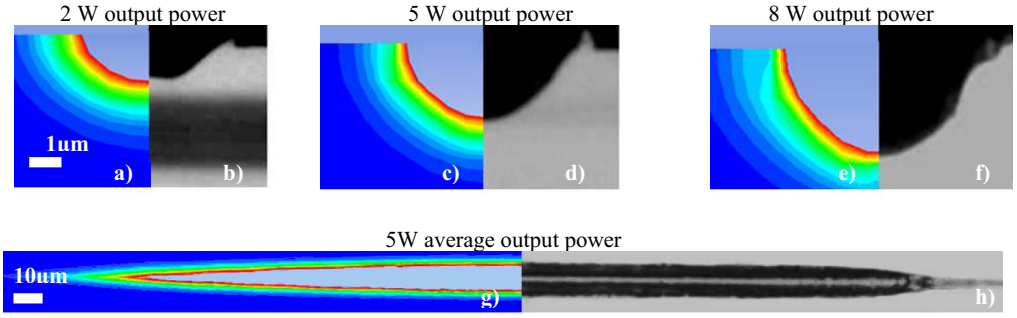

Fig. 4. Groove shape as a function of output power: (a),(c),(e),(g) simulation results; (b),(d),(f),(h) experimental results

As expected, the output power is significantly affecting the groove depth (Figs. 4 and 5). An increase of the laser power leads to an increase in heat surface flux, therefore, more material is evaporated and larger groove depths are achieved.

The simulation results obtained show good agreement with the experimental results (Fig. 5). The deviation form the experiments is within 10%. It is expected that the CFD model also predicts the final groove depth in the multi-pulse regime with the same accuracy.

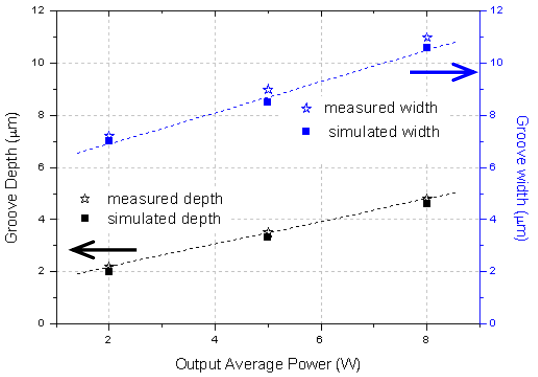

Fig. 5. Dependency of groove shape on output average power

5.2 Multi-pulse regime

Knowledge of single pulse behavior gives us the key for understanding of the multi-pulse cutting process. From the analytical point of view, for evaporation cutting the final depth is a function of depth pro pulse, scanning speed and beam shape.

To have a continuous affected profile in pulsed laser processing with a moving beam, the distance travelled by the beam during the pulse-off time should be small, i.e., there should be a large overlap between consecutive pulses. The schematic view of the overlapping phenomena is depicted in Fig. 6 where L is the beam length and d is the distance between pulses.

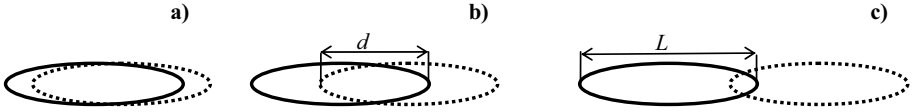

Fig. 6. Different overlapping phenomena in a moving beam pulsed laser process: (a) overlap with high overlapping degree; (b) overlap with lower overlapping degree; (c) overlap with the lowest overlapping degree

An analytical model for groove depth can be developed by assuming that the beam divergence is constant and that the work piece cools down to ambient temperature after each pulse (which has been verified by simulating the cooling phase). Then the final cutting depth can be approximated by:

$$z_n = z_1 N \tag{8}$$

where z_n is the depth cut by the nth pulse, z_1 is the single-pulse depth, and N is the number of pulses needed to reach the final depth. The latter depends on groove length of a single pulse L_{abl} and the distance between pulses d:

$$N = \frac{L_{abl}}{d} \tag{9}$$

The distance between pulses is the distance travelled during the pulse-off time and can be determined according to scanning speed V and pulse-off time t_{off} by:

$$d = V t_{off} \tag{10}$$

with:

$$t_{off} = \frac{1}{f} - t_{on} \tag{11}$$

where f is the frequency of the pulsed laser and t_{on} is the pulse duration (pulse-on) time.

According to Eq. (8) to Eq. (11), the groove depth does not increase anymore after N pulses (Eq. 9). Each additional pulse increases only the groove length.

To validate the analytical and CFD models experiments have been conducted. The size of the elliptical beam used was 6 x 460 µm. The work piece moved with a given velocity along the long beam axis. Fig. 7 shows the effect of output power and scanning speed on the final depth. Fig. 7d compares the analytical model with experiment and simulation.

The beam divergence measurement (Section 2) showed that the beam width divergence does not change drastically in a region from -20 to 20 µm. Therefore the divergence influence was neglected in the analytical calculation of groove depth using Eq. 8 and in the CFD modeling. The experiments show that this assumption is even valid for groove depths below 80 µm (Fig. 7d). Moreover, at higher cutting speed the distance in-between pulses increases causing a reduced final groove depth.

The analytical model can predict the groove depth, using single-pulse results (z_1, L_{abl}). Thus, scanning speed can be optimized, however, only for cutting depths below 80 µm. For depths above 80 µm the CFD model described in Section 4 should be used. This is also true when the information about complete groove geometry is needed because the analytical model can not predict groove width and length.

To validate the CFD model the case with 5 W output power, 600 mm/s cutting speed, 35 ns pulse duration at 10 kHz was simulated (Fig. 7d).

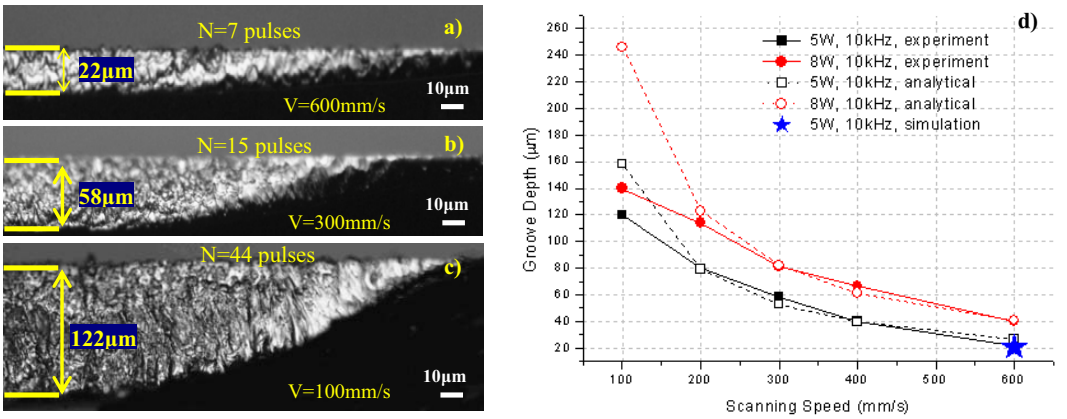

Fig. 7. (a),(b),(c) Experimental investigation of groove depth for multi-pulse cutting at 5 W average power; (d) comparison between experimental, analytical and simulation results

The simulated work-piece had a volume of 1400 x 30 x 10 µm with a mesh of average cell size of 1 µm. The generation of the new geometry based on the solution from the previous pulse and also the meshing of the new geometry after each pulse were performed manually. From Eq. (9) the total number of pulses needed to reach the final depth is 7-8. This was confirmed in the simulation in which the groove depth remained constant after 8 pulses. The simulation result is in good agreement with experiments (deviation 10%, Fig 7d). However, the procedure of manual geometry and mesh generation after each pulse is limited when the number of pulses exceeds, say, 20.

5.3 Effect of beam shape

Two Gaussian elliptical beams with various dimensions (Fig. 8) were investigated experimentally. The beam lengths were adjusted by changing the position of cylindrical lenses in the beam length adjustment unit of laser system (Fig. 1). The process parameters for this experiment are listed in Table 2.

Table 2. The process parameters used for experiments

Beam Width, µm	Beam Length, µm	Average Power, W	Scanning Speed, mm/s	Repetition Rate, kHz
6[2]	230[2] and 460[2]	4 and 6	100, 200, 300 and 400	10 ,15, 20 and 25

[2]value based on $1/e^2$-definition.

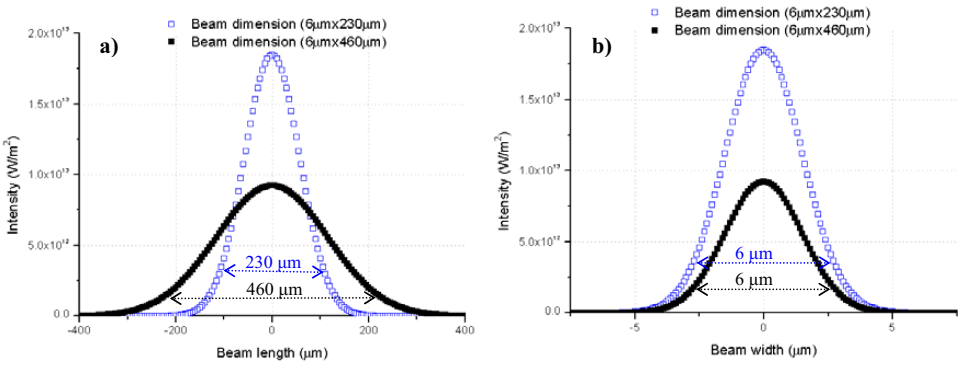

Fig. 8. Intensity of two elliptical beams at 5 W output power and 10 kHz repetition rate: (a) across long axis; (b) across short axis

Intensity distribution and overlapping degree depending on various laser parameters are calculated using Eqs. (1) and (2) and shown in Fig. 9. Because the energy per pulse decreases at higher repetition rate, intensity decreases as well. It is shown that at 10 kHz the intensity of the short beam is by a factor of two higher as that of the long beam (Fig. 9a). The overlapping degree increases with repetition rate and decreases with increasing scanning speed and decreasing laser beam dimension, here the length (Fig 9b).

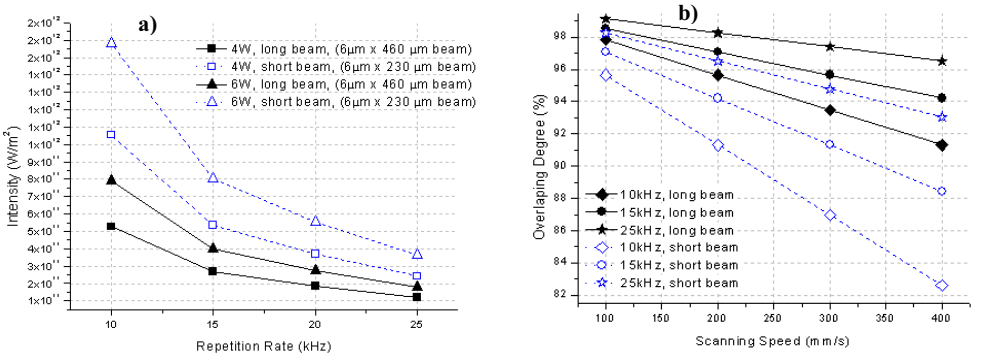

Fig. 9. (a) Intensity versus repetition rate; (b) overlapping degree versus scanning speed

By increasing the laser intensity value, which is defined as the peak power divided by the irradiated area, the total ablation rate increases as well (Fig. 10). The experimental results show that a deeper cut can be achieved with higher velocity and lower output power by using a short elliptical beam at higher repetition rates (25 kHz). By increasing repetition rate, the laser intensity decreases, but the overlapping degree increases. It is evidenced that the process with low laser intensity and high overlapping degree produces a deep cutting groove and at the same time a narrow groove width.

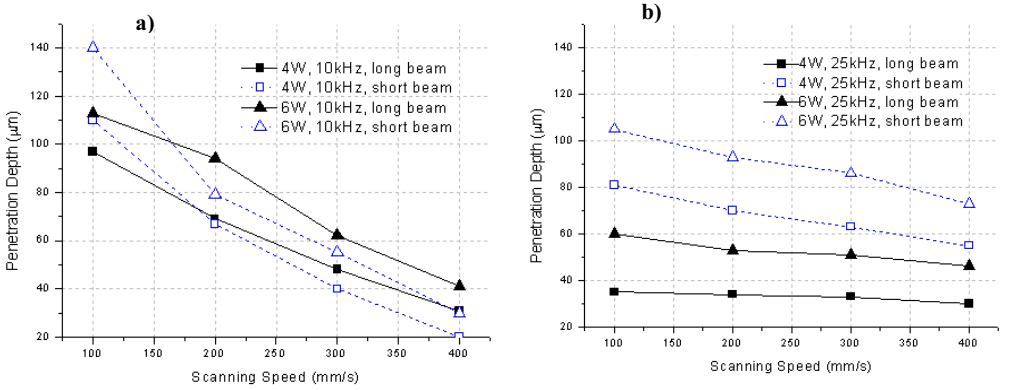

Fig. 10. Experimentally measured penetration depth at various scanning speeds and output powers at: (a) 10kHz; (b) 25kHz repetition rates

By cutting with the short beam at 10 kHz, the groove depth is close to but shallower than when cutting with the long beam (Figs. 10a and 11a, b). Because at 10 kHz, the short beam laser intensity is the largest measured (Fig. 9) the total heat generation is high. As a result, the groove becomes wider (Fig. 11a, b).

At higher repetition rate (25 kHz) the situation is completely different (Figs. 10b and 11c, d). In this case the

groove depth of cutting with the short beam is larger and widths are comparable to the results with the long beam.

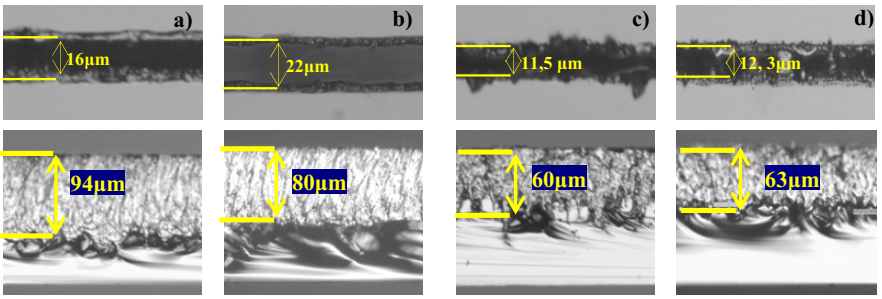

Fig. 11. Groove depth and width for: (a) long beam at 10 kHz, 6W, 200 mm/s; (b) short beam at 10 kHz, 6W, 200 mm/s; (c) long beam at 25 kHz, 6 W, 100 mm/s; (d) short beam at 25 kHz, 4W, 300 mm/s

The experiments demonstrated that by cutting with the short beam at 25 kHz, lower average power and higher scanning speed can be used to cut a deeper groove compared to cutting with the long beam. Hence, the higher intensity of the short beam dominates over lower overlapping degree.

The experimental results also show that the beam shape plays an important role for the resulting groove shape, and that an optimization of process parameters can improve the process considerably in terms of shorter cutting time and power consumption. Here, the short elliptical beam has a potential for deep, and fast cutting with low output power.

6. Conclusions

A number of experiments to study the effect of beam shape on cutting performance have been performed and a numerical model for single and multi-pulse laser cutting processes has been presented.

The experimental study has demonstrated the feasibility of UV laser cutting with various elliptical beams. It was shown that process optimization is needed for each beam and that the key factors for optimization are intensity and overlapping degree.

It has also been demonstrated that the numerical model predicts the single pulse groove shape well, and that multi-pulse cutting can be simulated when the final groove depth is reached within 20 pulses, a limitation is imposed by the manual geometry generation procedure described in Section 4. To overcome this limitation automation of the procedure is in progress.

References

1. D. Karnakis, J. Fieret, P. Rumsby, M. Gower, Microhole drilling using reshaped pulsed Gaussian beams (private correspondence).
2. A. Fell, S.Hopman, D.Kray. G. Wileke, Proceding of 22nd European Solar Energy Conference and Exhibition; Italy (2007).
3. Y. Zhang and A. Faghri, Int. J. Heat Mass Transfer 42 (1999) 1775.
4. Sundar Marimuthu, Computational Fluid Dynamic Analysis of Melting and Vaporization in Laser Cutting Process (private correspondence).
5. H. Kogelnik and T. Li, Appl. Opt. 5 (1966) 1550.
6. A. F. H. Kaplan, Appl. Phys. Lett. 70 (1997) 264.
7. M.A. Green and M. Keevers, Progress in Photovoltaics 3 (1995) 189.
8. Fluent, ANSYS FLUENT 12.0 User's Guide, April 2009 (www.fluent.com).